Refinement of future Arctic sea-ice projections

David Docquier (docquier.david@gmail.com)
Swedish Meteorological and Hydrological Institute https://orcid.org/0000-0002-5720-4253
Torben Koenigk
Swedish Meteorological and Hydrological Institute

Article

Keywords: Coupled Model Intercomparison Project 6, Northward Ocean Heat Transport, Summer Ice-free Conditions

Posted Date: March 9th, 2021

DOI: https://doi.org/10.21203/rs.3.rs-223865/v1

Version of Record: A version of this preprint was published at Communications Earth & Environment on July 15th, 2021. See the published version at https://doi.org/10.1038/s43247-021-00214-7.

Refinement of future Arctic sea-ice projections

David Docquier[1,*], Torben Koenigk[1,2]

[1]*Swedish Meteorological and Hydrological Institute, Rossby Centre, Norrköping, Sweden*

[2]*Bolin Centre for Climate Research, Stockholm University, Stockholm, Sweden*

** Correspondence: docquier.david@gmail.com*

Abstract

Arctic sea ice has been retreating at unprecedented pace over the past decades. Model projections show that the Arctic Ocean could be almost ice free in summer by the middle of this century. However, the uncertainties related to these projections are relatively large. Here we use 33 global climate models from the Coupled Model Intercomparison Project 6 (CMIP6) in order to reduce these uncertainties. We select the models that best capture the observed Arctic sea-ice area and volume and northward ocean heat transport to refine model projections of Arctic sea ice. This model selection leads to smaller Arctic sea-ice area and volume relative to the multi-model mean without model selection and summer ice-free conditions could occur as early as around 2035. These results highlight a potential underestimation of the future Arctic sea-ice loss when including all models.

Introduction

The retreat of Arctic sea ice is one of the most striking consequences of global warming and has strong implications for local and remote climate, biosphere and society[1]. The total area of the Arctic Ocean covered by sea ice, the Arctic sea-ice area, has decreased by about 2 million km^2 (yearly average) in the past 40 years of satellite observations, with more pronounced loss in the summer[1–3]. As sea ice has also thinned by 1.5 - 2 m in the Central Arctic since 1980[4,5], the total Arctic sea-ice volume has substantially decreased at a rate of 3800 km^3 per decade between 1979 and 2010[6]. The current Arctic sea-ice losses are strongly connected to the rising global temperatures[7–9], and thus to cumulative greenhouse gas emissions into the atmosphere[3,10]. Thus, the observed sensitivity of sea-ice changes to cumulative greenhouse gas emissions has been used to provide an estimate of the future Arctic sea-ice area[10].

However, this simple linear extrapolation strongly neglects non-linearities in the climate system and ocean-ice-atmosphere interactions and feedbacks[11,12], resulting in strong short- and long-term deviations from the ongoing negative trend in sea-ice area and volume[13]. In order to include these non-linearities and interactions, climate models can be used to provide more reliable projections of the fate of Arctic sea ice[14,15]. In particular, global climate models coupling the atmosphere, ocean and sea ice are well suited to make such projections[16–18]. The inclusion of these models in the different Coupled Model Intercomparison Project (CMIP) phases[19–21] allows to provide estimates of Arctic sea-ice area and volume projections in the next decades to centuries. The latest CMIP6 modelling effort[21] will feed into the next Intergovernmental Panel on Climate Change (IPCC) As-

sessment Report 6 and includes climate model projections that follow different greenhouse gas emission scenarios using the Shared Socioeconomic Pathways (SSPs)[22].

In our study, we use CMIP6 model outputs with the aim to reduce uncertainties in the future projections of Arctic sea ice. We select the models that best represent the present Arctic sea ice and northward ocean heat transport, as the latter is a major driver of the recent sea-ice loss, and we compare this model selection to the case without selection. We find that the sea-ice loss over this century is stronger using different model selection criteria compared to the average over all models without model selection. In particular, we find that summer ice-free Arctic conditions could occur as early as 2035 in the selection case, compared to 2061 in the no-selection case. We also find that some individual models strongly diverge from the multi-model mean and are associated with an outdated sea-ice model.

Results and discussion

Projections without model selection. In our study, we focus on both the high-emission SSP5-8.5 and low-emission SSP1-2.6 scenarios, which correspond to a global warming of around 4°C and 1°C, respectively, over this century (2081-2100 relative to 1995-2014)[23]. Averaged over 33 CMIP6 models (totalling 166 model members, Supplementary Table 1), the multi-model mean March Arctic sea-ice area and volume are reduced by 45 % and 78 %, respectively, in 2096-2100, compared to 2015-2019, in the high-emission scenario (Fig. 1a and Supplementary Fig. 3a). In September, the Arctic sea-ice area and volume are decreased by 90 % and 98 %, respectively, at

the end of the century (Fig. 1b and Supplementary Fig. 3b). The Arctic Ocean becomes almost ice free (sea-ice area lower than 1 million km^2 [12]) in September in 2061 for the multi-model mean (Fig. 1b). These Arctic sea-ice area and volume changes are considerably slowed down in the low-emission scenario: the multi-model mean March sea-ice area and volume are reduced by only 8 % and 28 %, respectively, at the end of the century, while the September sea-ice area is decreased by 49 % and thus never reaches almost ice-free conditions during this century, and the September sea-ice volume is lowered by 69 % (Supplementary Figs. 1 and 4).

However, such model projections suffer from large uncertainties related to the chosen greenhouse gas emission scenarios, model physics and internal variability[24]. Therefore, the spread in the future Arctic sea-ice projections is relatively large among climate models (Fig. 1 and Supplementary Fig. 1)[16,18]. In the high-emission scenario, the model spread increases over time for the March sea-ice area (Fig. 1a), while it decreases for the September sea-ice area as a large part of the models lose almost all their sea ice around 2050 (Fig. 1b). In the low-emission scenario, the model spread in March and September sea-ice area does not substantially vary over time as the changes over the twenty-first century are not as large as in the high-emission scenario (Supplementary Fig. 1).

Projections with model selection. Considering the simple average of all available models assumes that all models are equally plausible and that the range of their projections is representative of the uncertainty[25]. As some models better represent a specific aspect of the observed climate, e.g. Arctic sea ice in our case, we can argue that these models will provide more accurate projections of this specific aspect. A good agreement with observations does not constitute a final evidence

that the models are correct, but a bad agreement with such observations clearly indicates some problems of the models[25]. Different approaches have been taken to try to reduce the model spread in projections of Arctic sea-ice area for a given emission scenario. One such approach consists in giving a weight to each model based on its performance relative to observations during the historical period: models that strongly agree with observations receive more weight than models that poorly agree[23,25]. Another approach is to select models based on their historical performance and exclude models that do not satisfy the selection criteria[16,18,26].

In our study, we adopt the latter approach, i.e. model selection, as it allows to exclude model outliers that show large biases in relevant variables for the Arctic sea-ice representation based on clearly defined selection criteria. We define a series of selection criteria based on the mean, variability and trend in Arctic sea-ice area and volume (Methods). The northward Atlantic and Pacific ocean heat transports at different latitudes are also chosen as selection criteria as they have an important influence on the recent sea-ice changes[27–31]. These criteria are used to retain the CMIP6 models closest to observations over the historical period (1979-2014). This allows us to compute the multi-model means of Arctic sea-ice area and volume until the end of the twenty-first century based on the selected models, and thus to refine the model projections of Arctic sea-ice area and volume.

When applying our selection criteria, we find that the Arctic sea-ice area and volume generally reach smaller values at the end of this century compared to the case without selection, for both emission scenarios (Figs. 2-3 and Supplementary Figs. 2-5). This is mainly due to stronger

reductions in sea-ice area and volume over the twenty-first century in the selected models, and also to a smaller initial present-day Arctic sea-ice area to a lesser extent. The stronger reductions in sea-ice area and volume over the twenty-first century probably stem from the fact that the selected models have a larger sensitivity to anthropogenic global warming than the non-selected models[18]. Also, the smaller present-day sea-ice area in the selected models is due to the fact that the multi-model mean without selection overestimates the observed sea-ice area (Fig. 3a,b); thus, the selection of models closer to observations allows to reduce this overestimation, explaining the smaller present-day sea-ice area.

The loss in sea-ice area and volume over this century is most pronounced when selecting the models that best represent the historical Atlantic and Pacific ocean heat transports, in combination or not with the mean sea-ice area and volume (Figs. 2-3 and Supplementary Figs. 2-5). In the high-emission scenario and for all selection criteria including ocean heat transport, the March sea-ice area and volume reach less than 7 million km^2 and less than 5,000 km^3, respectively, by the end of the twenty-first century, and the September sea ice totally disappears (Fig. 3). Selecting the models that best represent the observed mean sea-ice area and volume and trend in sea-ice area also provides a stronger reduction in the future Arctic sea-ice area and volume compared to no selection, especially in September, but the sea-ice loss is less strong than with the ocean heat transport criterion (Figs. 2-3 and Supplementary Figs. 2-5).

The selection based on the variability in sea-ice area and volume and trend in sea-ice volume is not as clear-cut: depending on the month or the scenario, these selection criteria provide smaller

or larger reductions in sea-ice area and volume (Figs. 2-3 and Supplementary Figs. 2-5). For sea-ice area and volume variability, this is partly linked to the fact that these quantities are directly related to atmospheric variability[9]. In turn, the latter does not highly depend on the total amount of ice. Thus, even a model with too much (or not enough) sea ice can have a realistic atmospheric variability, leading to a realistic sea-ice variability.

An additional model selection criterion that we include in our analysis is the minimum number of ensemble members. We select all models that have at least five members, as this allows to both keep the models that take into account the uncertainty linked to internal variability and to have about a third of the total number of models. We find that the multi-model mean averaged over these models also leads to a stronger sea-ice loss relative to no selection, with no remaining sea ice in September by the end of the century and reductions of 60% and 87% in March sea-ice area and volume, respectively, in the high-emission scenario (Figs. 2-3). This strengthens our main finding that the reduction in sea ice is stronger with model selection.

Our model selection based on the historical performance allows to exclude outliers that have either too much or not enough Arctic sea ice. For the winter months, outliers are mainly located on the high end as most models overestimate the observed sea-ice area (Fig. 3a), while for the summer months, outliers are located on either end (Fig. 3b)[18]. Thus, our model selection allows to narrow down the spread in model projections of Arctic sea ice by excluding outliers. In particular, the threshold of an ice-free Arctic in summer is reached much earlier with model selection compared to without selection. In the high-emission scenario, four selection criteria including the ocean

heat transport provide an ice-free Arctic in September as early as in the range 2034-2037, while only one selection criterion (sea-ice area variability) provides an ice-free Arctic some years after the multi-model mean without selection (Figs. 2b-3b). In the low-emission scenario, the selection criteria including ocean heat transport and the number of members all provide an ice-free Arctic in September for at least some years before the end of this century, but with a sea-ice area staying close to the 1 million km^2 threshold until the end of the century (Supplementary Fig. 2b).

Ocean components in CMIP6 models. The 33 CMIP6 models used here include 10 different ocean components. Grouping the different models by ocean component and computing the associated multi-model mean sea-ice area, we find that the models that include the LICOM, MICOM, INM-OM and MOM ocean components have larger March and September sea-ice areas over the twenty-first century compared to the multi-model mean averaged over all models for the two emission scenarios (Fig. 4a and Supplementary Figs. 6a-8a). The models sharing the other six ocean components generally show a smaller sea-ice area during the twenty-first century, with the exception of MPIOM, MRI.COM and FESOM in March at the end of the century.

As the NEMO and MOM components are both shared by more than five different CMIP6 models, we further investigate the individual models using these two ocean components. This reveals that the multi-model mean sea-ice area associated with these two ocean components is clearly driven by specific outliers. The below-average March sea-ice area from NEMO in the high-emission scenario is driven by two CMIP6 models that have a very low sea-ice area over the whole twenty-first century (Fig. 4b). It is worth noting that these two models use version 2 of the

Louvain-la-Neuve sea Ice Model (LIM2), which is a former version of the LIM3 sea-ice model[32]. In particular, LIM2 only includes one sea-ice thickness category, while LIM3 has five thickness categories, making it more reliable in terms of sea-ice area variability compared to observations[33]. Four other models using NEMO have a strong reduction in March sea-ice area in the high-emission scenario at the end of the twenty-first century (Fig. 4b).

The above-average March sea-ice area from MOM in the high-emission scenario is driven by one specific CMIP6 sea-ice model that has a sea-ice area about 4 million km^2 larger than the MOM multi-model mean (Fig. 4b); this is also the case in the low-emission scenario (Supplementary Fig. 6b). This specific model includes version 1 of the Sea Ice Simulator (SIS1) from the Geophysical Fluid Dynamics Laboratory (GFDL), which is a former version of the SIS2 sea-ice model[34]. The SIS2 model has a number of supplementary features that improve upon SIS1, including a Delta-Eddington radiation scheme, revised thermodynamic algorithms, and a C-grid discretization allowing improved representation of ice transport through narrow channels.

In September and for the two emission scenarios, the above-average sea-ice area from MOM is driven by two specific models, which both use the SIS1 sea-ice model (Supplementary Figs. 7b-8b). During the same month, three models using the NEMO ocean component show a very low sea-ice area at the beginning of the twenty-first century (Supplementary Figs. 7b-8b). These three models do not share the same sea-ice model (either CICE or LIM3), but they do not show such a large departure from the NEMO multi-model mean compared to the previously identified NEMO and MOM outliers. Thus, we argue that part of the relatively small (large) sea-ice area through

the twenty-first century simulated by CMIP6 models using the NEMO (MOM, respectively) ocean component is due to an outdated sea-ice model (LIM2 for NEMO and SIS1 for MOM). That is certainly not the only reason, but further investigation would be needed to understand the role of the ocean and sea-ice components in the future projections.

Summary and outlook. The future projections of Arctic sea ice can potentially be improved by selecting the climate models that best represent the present state in terms of sea-ice area, sea-ice volume and northward ocean heat transport. This model selection reveals that the sea-ice area and volume reach lower values at the end of this century compared to the multi-model mean without selection. This arises both from a more rapid reduction in these quantities through this century and from a lower present-day sea-ice area. Using such a model selection, the timing of an almost ice-free Arctic in summer is advanced by up to 25 years in the high-emission scenario, i.e. it could occur as early as 2035. Thus, these results highlight a potential underestimation of the future Arctic sea-ice loss when including all models.

The rapid ongoing disintegration of Arctic sea ice can have dramatic consequences on other components of the climate system, such as the atmosphere[35,36] and the ocean[37,38], as well as the biosphere and our societies[1]. Thus, it is highly important to accurately monitor the current Arctic sea-ice changes and to improve its future model projections. As the number of models included in climate model intercomparisons is constantly rising, there is more and more room for using sophisticated methods that provide a best estimate of future changes in sea ice. This study intends to encourage such initiatives in order to reduce the uncertainties in model projections of Arctic sea

ice.

Methods

CMIP6 model simulations. In our study, we analysed the outputs from the climate models participating in the Coupled Model Intercomparison Project 6 (CMIP6) effort[21]. We extracted the monthly mean sea-ice concentration and sea-ice volume per area (or sea-ice thickness if the sea-ice volume per area was not available) from the CMIP6 models that were run over both the historical period (1850-2014) and the future (2015-2100), using the two Shared Socioeconomic Pathways SSP1-2.6 (weak greenhouse gas emission scenario), and SSP5-8.5 (strong emission scenario). We computed the total Arctic sea-ice area as the product of sea-ice concentration and grid-cell area summed over the ocean region north of 40°N. The total Arctic sea-ice volume is the product of sea-ice volume per area (or sea-ice thickness times sea-ice concentration) and grid-cell area summed over the ocean region north of 40°N. Sea-ice area from 32 models is used for the SSP1-2.6 scenario and from 33 models for the SSP5-8.5 scenario (Supplementary Table 1). As some models have run several ensemble members with different initial conditions, we have a total of 166 model simulations for both SSP1-2.6 and SSP5-8.5. Sea-ice volume from 28 models is used for both SSP1-2.6 and SSP5-8.5, including a total of 155 member simulations for SSP1-2.6 and 154 member simulations for SSP5-8.5. Additionally, we extracted the monthly mean historical northward ocean heat transport (computed online by the different models) from 16 models (it was not available for the other models). In our analyses, we computed the ensemble mean sea-ice area, sea-ice volume and ocean heat transport over all members for each individual model. Supplementary Table 1 provides

the number of ensemble members available for each model and each variable.

Reference products. In order to evaluate the CMIP6 models over the historical period, we used different observational and reanalysis datasets. For sea-ice area, we retrieved the sea-ice concentration from the European Organisation for the Exploitation of Meteorological Satellites (EUMETSAT) Ocean Sea Ice Satellite Application Facility (OSI SAF)[39] available since 1979, and we integrated this quantity over the northern hemisphere (north of 40°N). We used the sea-ice volume from the Pan-Arctic Ice-Ocean Modeling and Assimilation System (PIOMAS)[40], which is a coupled ocean - sea ice model with capability of assimilating daily sea-ice concentration and sea-surface temperature. This dataset is available since 1979 and shows reasonable agreement with observations[41]. The estimates of ocean meridional heat transport (Atlantic and Pacific) come from Trenberth et al. (2019)[42] and are deduced from top-of-atmosphere radiation coming from Clouds and the Earth's Radiant Energy System (CERES), vertically-integrated atmospheric energy divergence from ERA-Interim, and ocean heat content from Ocean Reanalysis System 5 (ORAS5). This data set is available for the period 2000-2016. Finally, we also used the Atlantic Ocean heat transport estimates derived from the Rapid Climate Change Meridional Overturning Circulation and Heatflux Array (RAPID-MOCHA) observing system deployed at 26°N (2004-2018)[43], as well as from the Overturning in the Subpolar North Atlantic Program (OSNAP) observing system deployed around 57°N (2014 and 2016)[44].

Selection criteria. In order to retain the CMIP6 models closest to observations and reanalysis over the historical period, we defined a series of selection criteria based on sea-ice area, sea-ice volume and ocean heat transport. Here is a description of these selection criteria:

1. Mean sea-ice area: we selected the 15 models (about half of the available models) closest to the observed mean sea-ice area averaged over 1979-2014 for both March and September combined.

2. Mean sea-ice volume: same as criterion 1 for sea-ice volume.

3. Sea-ice area variability: we selected the 15 models closest to the observed detrended standard deviation in sea-ice area over 1979-2014 for both March and September combined.

4. Sea-ice volume variability: same as criterion 3 for sea-ice volume.

5. Trend in sea-ice area: we selected the 15 models closest to the observed trend in sea-ice area over 1979-2014 for both March and September combined.

6. Trend in sea-ice volume: same as criterion 5 for sea-ice volume.

7. Atlantic ocean heat transport ('Atlantic OHT' in the figure legends): we selected the 8 models (half of the models having ocean heat transport) closest to the observed mean Atlantic ocean heat transport at both 26°N and 57°N combined, averaged over 2000-2014. As the OSNAP measurements at 57°N only cover 2014 and 2016, we used the mean of these two years for the observed mean value at this latitude.

8. Atlantic and Pacific ocean heat transports ('Atl/Pac OHT' in the figure legends): we selected the 8 models closest to the observed mean ocean heat transport at both 70°N in the Atlantic Ocean and 60°N in the Pacific Ocean (combined), averaged over 2000-2014.

9. Atlantic ocean heat transport and mean sea-ice area ('Atlantic OHT + sea-ice area' in the figure legends): we selected the 8 models better satisfying both criteria 7 and 1.

10. Atlantic and Pacific ocean heat transports and mean sea-ice area ('Atl/Pac OHT + sea-ice area' in the figure legends): we selected the 8 models better satisfying both criteria 8 and 1.

11. Atlantic ocean heat transport and mean sea-ice volume ('Atlantic OHT + sea-ice volume' in the figure legends): we selected the 8 models better satisfying both criteria 7 and 2.

12. Atlantic and Pacific ocean heat transports and mean sea-ice volume ('Atl/Pac OHT + sea-ice volume' in the figure legends): we selected the 8 models better satisfying both criteria 8 and 2.

We defined a last criterion based on the number of members per model ('$\geq$ 5 members' in the figure legends): we retained only the models that have at least 5 ensemble members (10 models in total).

Data availability

All the CMIP6 model data used in this study (historical and scenario runs) can be accessed through the ESGF nodes: `https://esgf-node.llnl.gov/search/cmip6`. The observed sea-ice concentration from OSI SAF[39] can be accessed through the EUMETSAT repository: `http://dx.doi.org/10.15770/EUM_SAF_OSI_0008`. The PIOMAS[40] sea-ice volume data can be accessed via the Polar Science Center of the University of Washington: `http://psc.apl.uw.`

edu/research/projects/arctic-sea-ice-volume-anomaly. The ocean meridional heat transport estimates from Trenberth et al. (2019)[42] are located here: https://doi.org/10.5065/9v3y-fn61. The RAPID-MOCHA[43] ocean heat transport at 26.5°N can be retrieved from the Rosenstiel School Ocean Technology Lab: https://mocha.rsmas.miami.edu/mocha/results/index.html. The OSNAP[44] ocean heat transport data can accessed here: https://www.o-snap.org/observations/data.

Code availability

The Python scripts to produce the figures of this article are available on Zenodo: https://zenodo.org/record/4454860.

References

1. IPCC. *Summary for Policymakers. In: IPCC Special Report on the Ocean and Cryosphere in a Changing Climate [H.-O. Pörtner, D.C. Roberts, V. Masson-Delmotte, P. Zhai, M. Tignor, E. Poloczanska, K. Mintenbeck, M. Nicolai, A. Okem, J. Petzold, B. Rama, N. Weyer (eds.)]* (2019). Cambridge University Press, Cambridge, United Kingdom and New York, NY, USA.

2. Onarheim, I. H., Eldevik, T., Smedsrud, L. H. & Stroeve, J. C. Seasonal and regional manifestation of Arctic sea ice loss. *Journal of Climate* **31**, 4917–4932 (2018).

3. Stroeve, J. & Notz, D. Changing state of Arctic sea ice across all seasons. *Environmental Research Letters* **13** (2018).

4. Lindsay, R. & Schweiger, A. Arctic sea ice thickness loss determined using subsurface, aircraft, and satellite observations. *The Cryosphere* **9**, 269–283 (2015).

5. Kwok, R. Arctic sea ice thickness, volume, and multiyear ice coverage: losses and coupled variability (1958-2018). *Environmental Research Letters* **13** (2018).

6. Schweiger, A., Wood, K. R. & Zhang, J. Arctic sea ice volume variability over 1901-2010: A model-based reconstruction. *Journal of Climate* **32**, 4731–4752 (2019).

7. Mahlstein, I. & Knutti, R. September Arctic sea ice predicted to disappear for 2°C global warming above present. *Journal of Geophysical Research* **117**, D06104 (2012).

8. Niederdrenk, A. L. & Notz, D. Arctic sea ice in a 1.5°C warmer world. *Geophysical Research Letters* **45**, 1963–1971 (2018).

9. Olonscheck, D., Mauritsen, T. & Notz, D. Arctic sea-ice variability is primarily driven by atmospheric temperature fluctuations. *Nature Geoscience* **12**, 430–434 (2019).

10. Notz, D. & Stroeve, J. Observed Arctic sea-ice loss directly follows anthropogenic CO2 emission. *Science* **354**, 747–750 (2016).

11. Goosse, H. *et al.* Quantifying climate feedbacks in polar regions. *Nature Communications* **9** (2018).

12. Notz, D. & Stroeve, J. The trajectory towards a seasonally ice-free Arctic Ocean. *Current Climate Change Reports* **4**, 407–416 (2018).

13. Simmonds, I. & Rudeva, I. The great Arctic cyclone of August 2012. *Geophysical Research Letters* **39**, L23709 (2012).

14. Jahn, A., Kay, J. E., Holland, M. M. & Hall, D. M. How predictable is the timing of a summer ice-free Arctic? *Geophysical Research Letters* **43**, 9113–9120 (2016).

15. Screen, J. A. & Deser, C. Pacific Ocean variability influences the time of emergence of a seasonally ice-free Arctic Ocean. *Geophysical Research Letters* **46**, 2222–2231 (2019).

16. Massonnet, F. *et al.* Constraining projections of summer Arctic sea ice. *The Cryosphere* **6**, 1383–1394 (2012).

17. Davy, R. & Outten, S. The Arctic surface climate in CMIP6: Status and developments since CMIP5. *Journal of Climate* **33**, 8047–8068 (2020).

18. SIMIP Community. Arctic sea ice in CMIP6. *Geophysical Research Letters* **47**, e2019GL086749 (2020).

19. Meehl, G. A. *et al.* The WCRP CMIP3 multimodel dataset. *Bulletin of the American Meteorological Society* 1383–1394 (2007).

20. Taylor, K. E., Stouffer, R. J. & Meehl, G. A. An overview of CMIP5 and the experiment design. *Bulletin of the American Meteorological Society* 485–498 (2013).

21. Eyring, V. *et al.* Overview of the Coupled Model Intercomparison Project Phase 6 (CMIP6) experimental design and organization. *Geoscientific Model Development* **9**, 1937–1958 (2016).

22. O'Neill, B. C. *et al.* The Scenario Model Intercomparison Project (ScenarioMIP) for CMIP6. *Gescientific Model Development* **9**, 3461–3482 (2016).

23. Brunner, L. *et al.* Reduced global warming from CMIP6 projections when weighting models by performance and independence. *Earth System Dynamics* **11**, 995–1012 (2020).

24. Hawkins, E. & Sutton, R. The potential to narrow uncertainty in regional climate predictions. *Bulletin of the American Meteorological Society* **90**, 1095–1107 (2009).

25. Knutti, R. *et al.* A climate model projection weighting scheme accounting for performance and interdependence. *Geophysical Research Letters* **44**, 1909–1918 (2017).

26. Wang, M. & Overland, J. E. A sea ice free summer arctic within 30 years: An update from cmip5 models. *Geophysical Research Letters* **39**, L18501 (2012).

27. Holland, M. M., Bitz, C. M. & Tremblay, B. Future abrupt reductions in the summer Arctic sea ice. *Geophysical Research Letters* **33**, L23503 (2006).

28. Arthun, M., Eldevik, T., Smedsrud, L. H., Skagseth, O. & Ingvaldsen, R. B. Quantifying the influence of Atlantic heat on Barents Sea ice variability and retreat. *Journal of Climate* **25**, 4736–4743 (2012).

29. Polyakov, I. V. *et al.* Greater role for Atlantic inflows on sea-ice loss in the Eurasian Basin of the Arctic Ocean. *Science* **356**, 285–291 (2017).

30. Serreze, M. C., Barrett, A. P., Crawford, A. D. & Woodgate, R. A. Monthly variability in Bering Strait oceanic volume and heat transports, links to atmospheric circulation and ocean

temperature, and implications for sea ice conditions. *Journal of Geophysical Research* **124**, 9317–9337 (2019).

31. Docquier, D., Koenigk, T., Fuentes-Franco, R., Karami, M. P. & Ruprich-Robert, Y. Impact of ocean heat transport on the Arctic sea-ice decline: a model study with EC-Earth3. *Climate Dynamics* (2021).

32. Rousset, C. *et al.* The Louvain-La-Neuve sea ice model LIM3.6: global and regional capabilities. *Geoscientific Model Development* **8**, 2991–3005 (2015).

33. Massonnet, F. *et al.* On the influence of model physics on simulations of Arctic and Antarctic sea ice. *The Cryosphere* **5**, 687–699 (2011).

34. Adcroft, A. *et al.* The GFDL Global Ocean and Sea Ice Model OM4.0: Model description and simulation features. *Journal of Advances in Modeling Earth Systems* **11**, 3167–3211 (2019).

35. Overland, J. E. & Wang, M. Large-scale atmospheric circulation changes are associated with the recent loss of Arctic sea ice. *Tellus A* **62**, 1–9 (2010).

36. Dai, A., Luo, D., Song, M. & Liu, J. Arctic amplification is caused by sea-ice loss under increasing CO2. *Nature Communications* **10** (2019).

37. Bhatt, U. S. *et al.* Implications of Arctic sea ice decline for the Earth System. *Annual Review Environment Resources* **39**, 57–89 (2014).

38. Sévellec, F., Federov, A. V. & Liu, W. Arctic sea-ice decline weakens the Atlantic Meridional Overturning Circulation. *Nature Climate Change* **7**, 604–610 (2017).

366 39. Lavergne, T. *et al.* Version 2 of the EUMETSAT OSI SAF and ESA CCI sea-ice concentration
367 climate data records. *The Cryosphere* **13**, 49–78 (2019).

368 40. Zhang, J. & Rothrock, D. A. Modeling global sea ice with a thickness and enthalpy distribution
369 model in generalized curvilinear coordinates. *Monthly Weather Review* **131**, 845–861 (2003).

370 41. Schweiger, A. *et al.* Uncertainty in modeled Arctic sea ice volume. *Journal of Geophysical*
371 *Research* **116**, C00D06 (2011).

372 42. Trenberth, K. E., Zhang, Y., Fasullo, J. T. & Cheng, L. Observation-based estimates of global
373 and basin o0cean meridional heat transport time series. *Journal of Climate* **32**, 4567–4583
374 (2019).

375 43. Johns, W. E. *et al.* Continuous, array-based estimates of Atlantic Ocean heat transport at
376 26.5N. *Journal of Climate* **24**, 2429–2449 (2011).

377 44. Lozier, M. S. *et al.* A sea change in our view of overturning in the subpolar North Atlantic.
378 *Science* **363**, 516–521 (2019).

379 **Acknowledgements**

380 D.D. was supported by the OSeaIce project (https://cordis.europa.eu/project/id/834493), which has
381 received funding from the European Unions Horizon 2020 research and innovation programme
382 under the Marie Sklodowska-Curie grant agreement No. 834493. T.K. was supported by the
383 NordForsk-funded Nordic Centre of Excellence project (award 76654) Arctic Climate Predic-

tions: Pathways to Resilient, Sustainable Societies (ARCPATH). We thank K. Zimmermann and M. Sahlin for retrieving the CMIP6 data onto the SMHI servers.

Author contributions

D.D. led the work with contributions from T.K. DD performed the computations, analysed the results, produced the figures and led the paper writing. T.K. participated in the design of the study, the interpretation of the results and the writing of the paper.

Competing interests

The authors declare no competing interests.

Additional information

Supplementary information is available for this paper.

Correspondence and request for materials should be addressed to D.D.

Figures

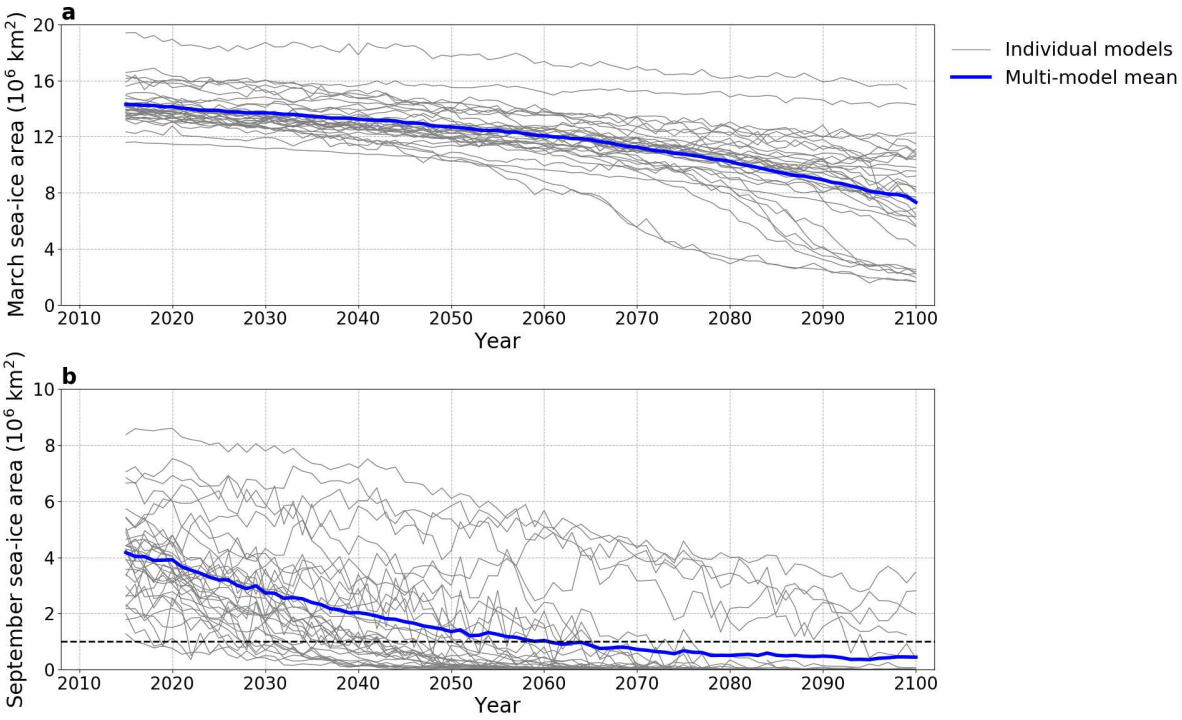

Figure 1: Evolution of future Arctic sea-ice area in (a) March and (b) September for the CMIP6 individual models (thin gray curves) and the multi-model mean (thick blue curve), based on the SSP5-8.5 scenario.

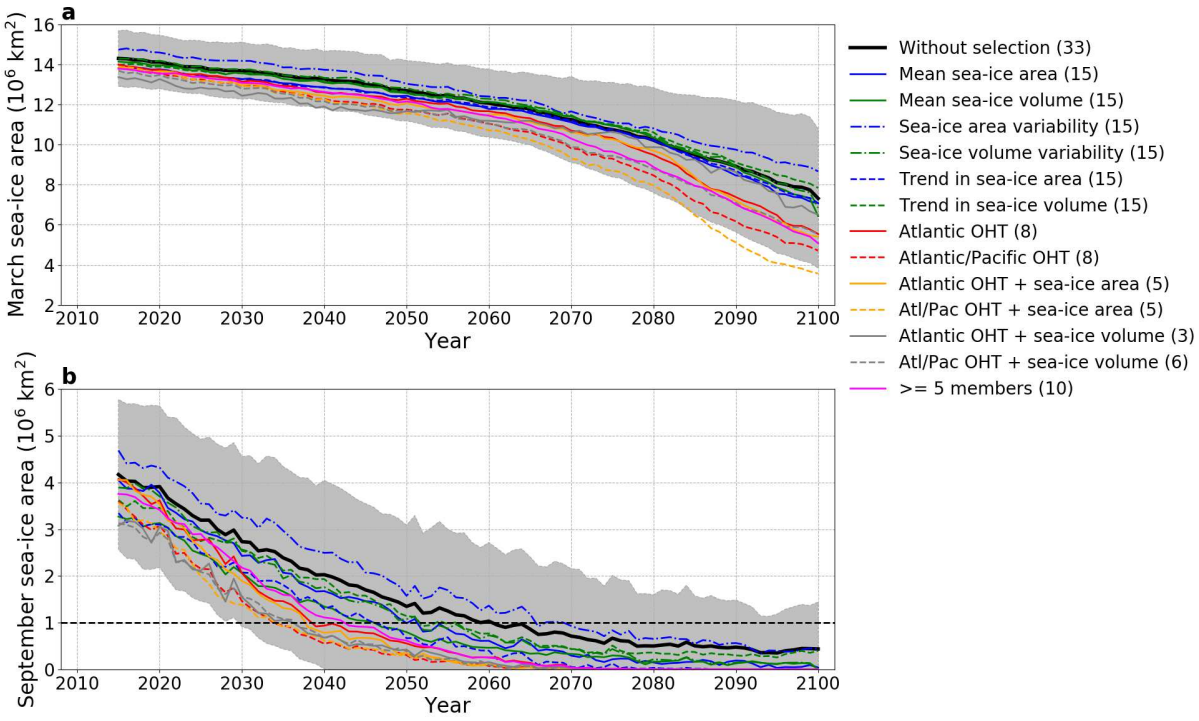

Figure 2: Evolution of future Arctic sea-ice area in (a) March and (b) September for the multi-model mean averaged over all models (thick black curve) and averaged over the models selected according to different criteria (coloured curves), based on the SSP5-8.5 scenario. The gray shading is the standard deviation around the multi-model mean without selection. The number of models included in each multi-model averaging is indicated in brackets in the legend.

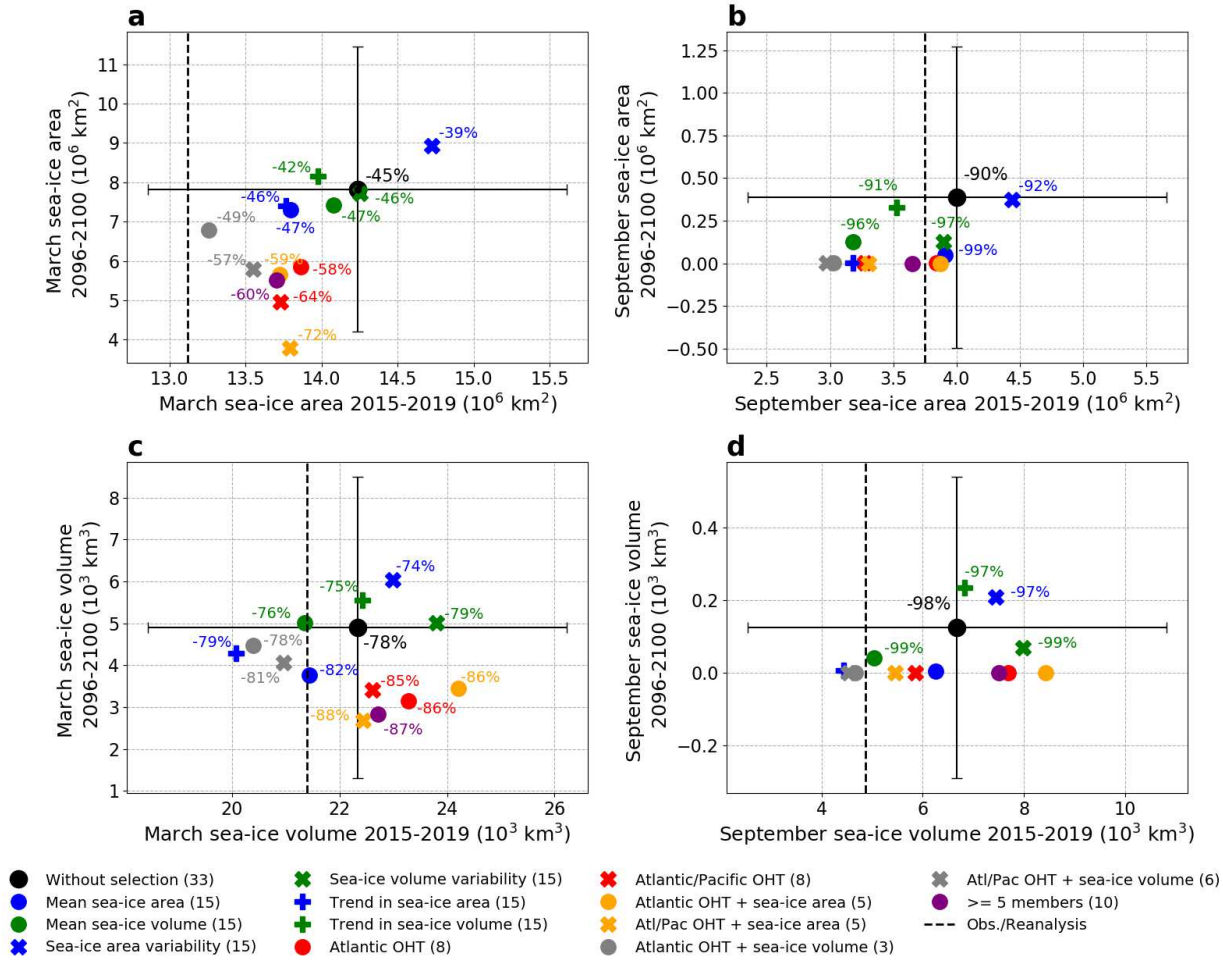

Figure 3: (a) March Arctic sea-ice area in 2096-2100 against 2015-2019 for the multi-model mean averaged over all models (black dot, with the ensemble standard deviation as error bars) and the multi-models means averaged over the models selected according to different criteria (coloured dots and crosses), based on the SSP5-8.5 scenario. (b) Same as (a) for the September Arctic sea-ice area. (c) Same as (a) for the March Arctic sea-ice volume. (d) Same as (a) for the September Arctic sea-ice volume. The relative change in sea-ice area / volume between 2015-2019 and 2096-2100 is shown beside the different items (not indicated if the change is -100 %). The dashed vertical lines show (a-b) the sea-ice area from OSI SAF observations and (c-d) sea-ice volume from PIOMAS reanalysis in 2015-2019. The number of models included in each multi-model averaging is indicated in brackets in the legend.

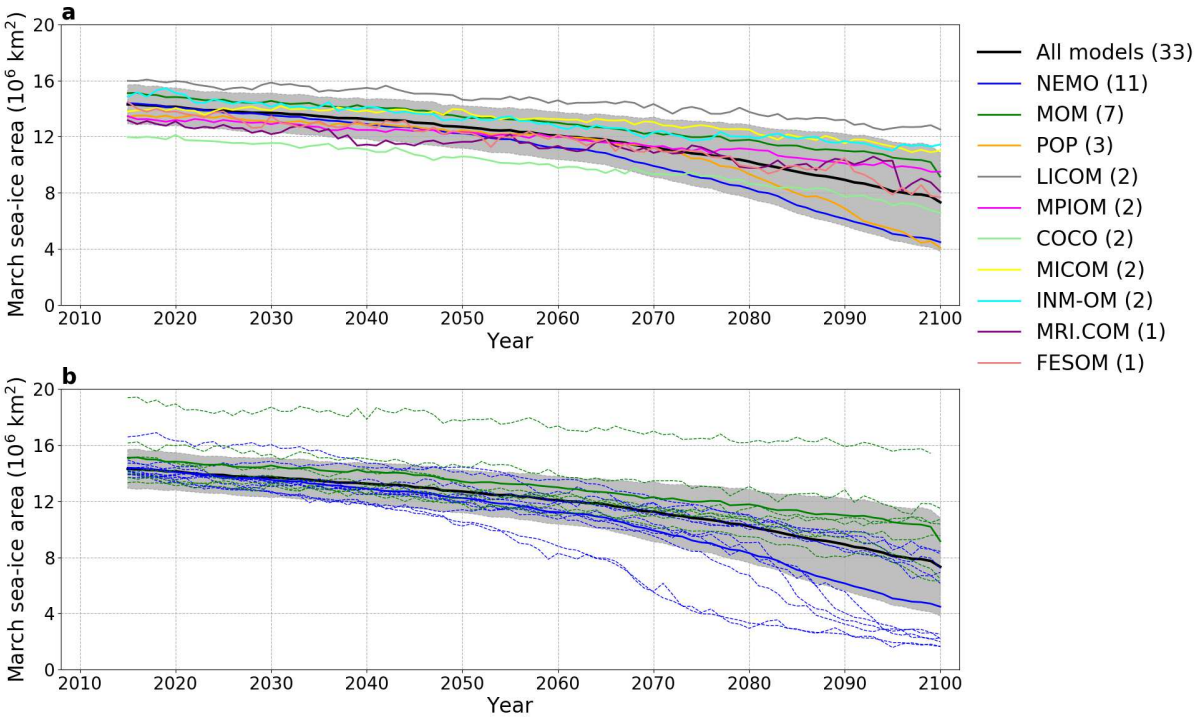

Figure 4: (a) Evolution of future March Arctic sea-ice area for the multi-model mean averaged over all models (thick black curve) and averaged over all models including the same ocean component (coloured curves), based on the SSP5-8.5 scenario. (b) Same as (a) but with only the multi-model means averaged over models including the NEMO (solid blue) and MOM (solid green) ocean components, as well as the individual NEMO and MOM models represented as dashed blue and green lines, respectively. The gray shading is the standard deviation around the multi-model mean without selection. The number of models included in each multi-model averaging is indicated in brackets in the legend.

Figures

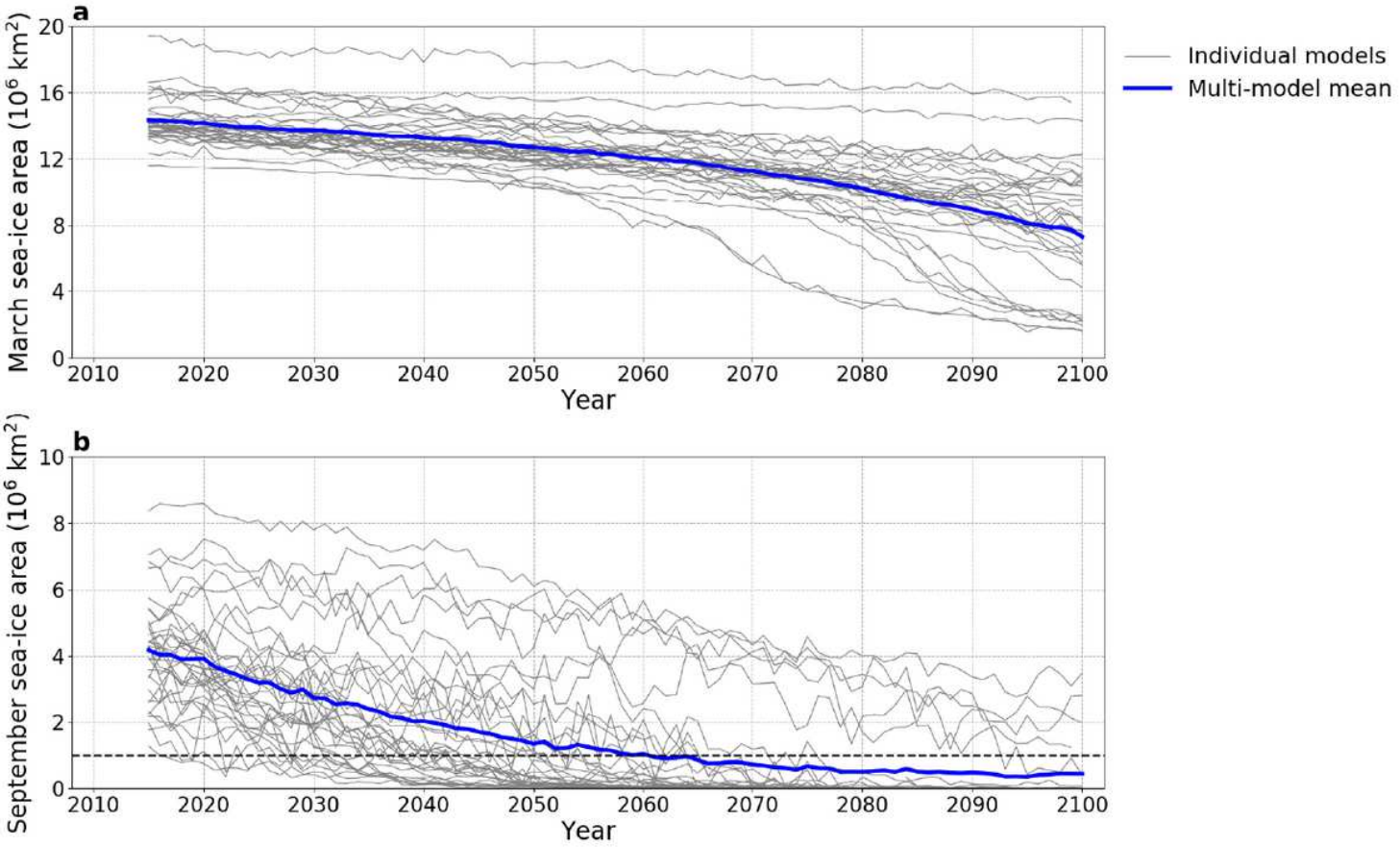

Figure 1

Evolution of future Arctic sea-ice area in (a) March and (b) September for the CMIP6 individual models (thin gray curves) and the multi-model mean (thick blue curve), based on the SSP5-8.5 scenario.

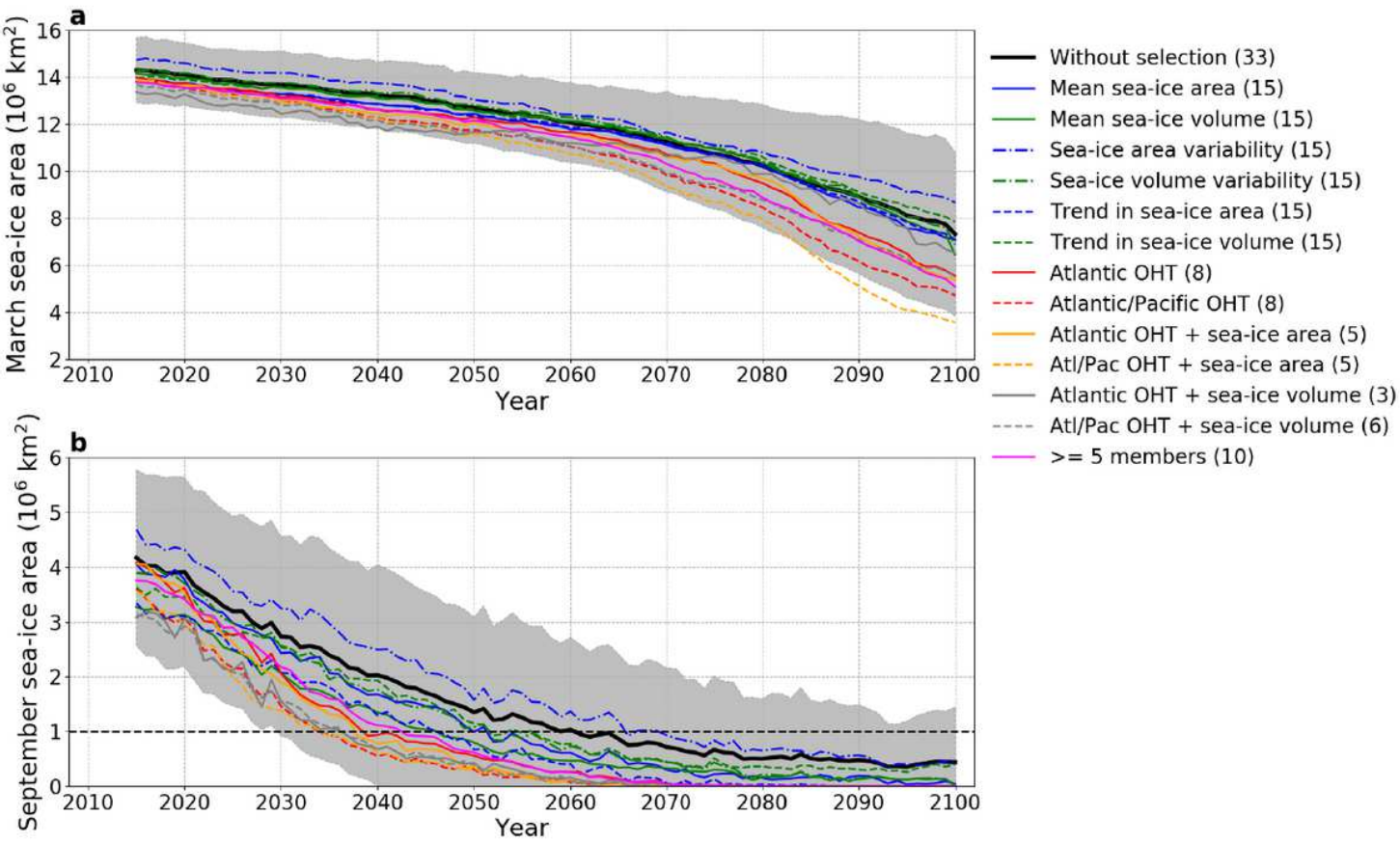

Figure 2

Evolution of future Arctic sea-ice area in (a) March and (b) September for the multi-model mean averaged over all models (thick black curve) and averaged over the models selected according to different criteria (coloured curves), based on the SSP5-8.5 scenario. The gray shading is the standard deviation around the multi-model mean without selection. The number of models included in each multi-model averaging is indicated in brackets in the legend.

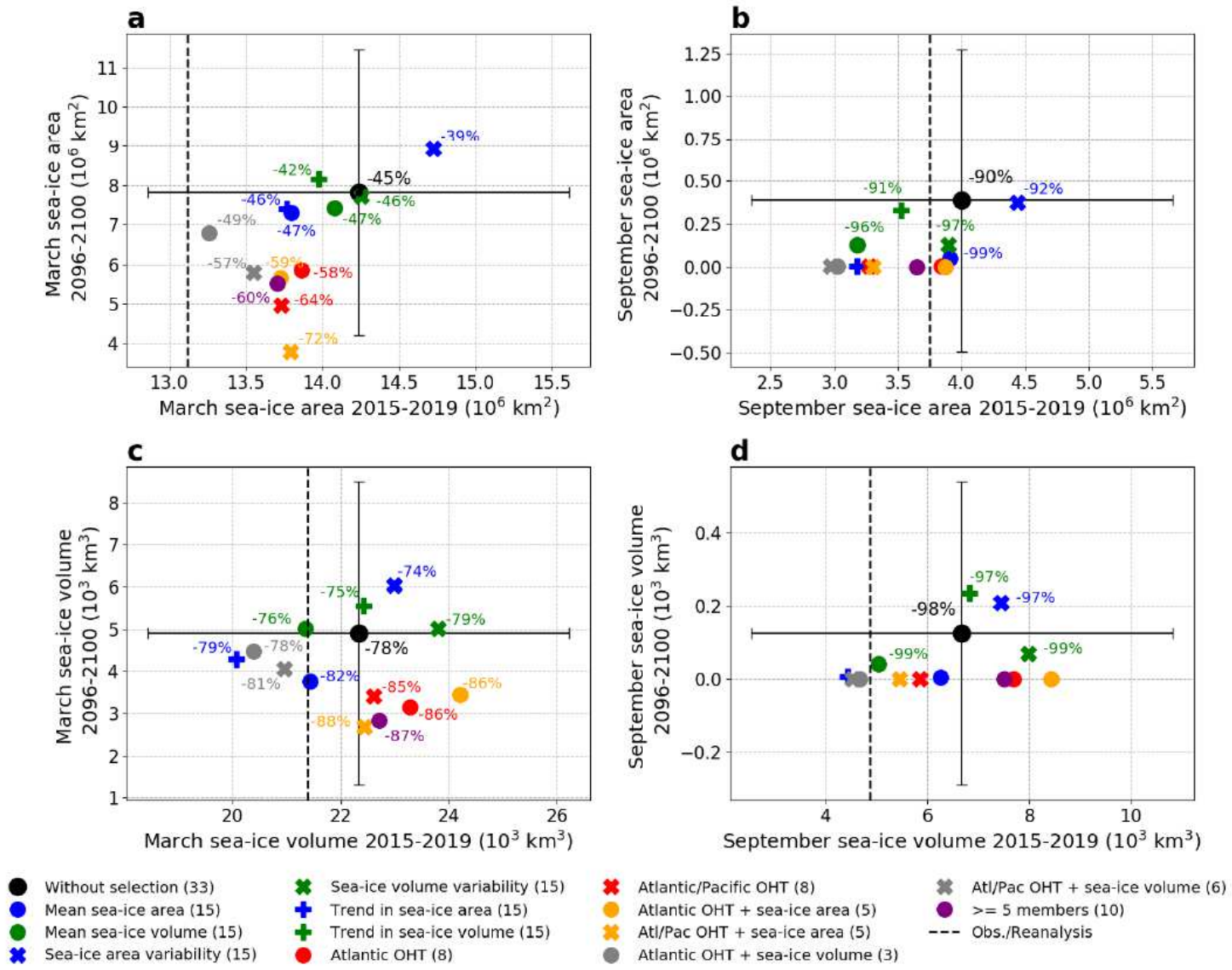

Figure 3

(a) March Arctic sea-ice area in 2096-2100 against 2015-2019 for the multi-model mean averaged over all models (black dot, with the ensemble standard deviation as error bars) and the multi-models means averaged over the models selected according to different criteria (coloured dots and crosses), based on the SSP5-8.5 scenario. (b) Same as (a) for the September Arctic sea-ice area. (c) Same as (a) for the March Arctic sea-ice volume. (d) Same as (a) for the September Arctic sea-ice volume. The relative change in sea-ice area / volume between 2015-2019 and 2096-2100 is shown beside the different items (not indicated if the change is -100 %). The dashed vertical lines show (a-b) the sea-ice area from OSI SAF observations and (c-d) sea-ice volume from PIOMAS reanalysis in 2015-2019. The number of models included in each multi-model averaging is indicated in brackets in the legend.

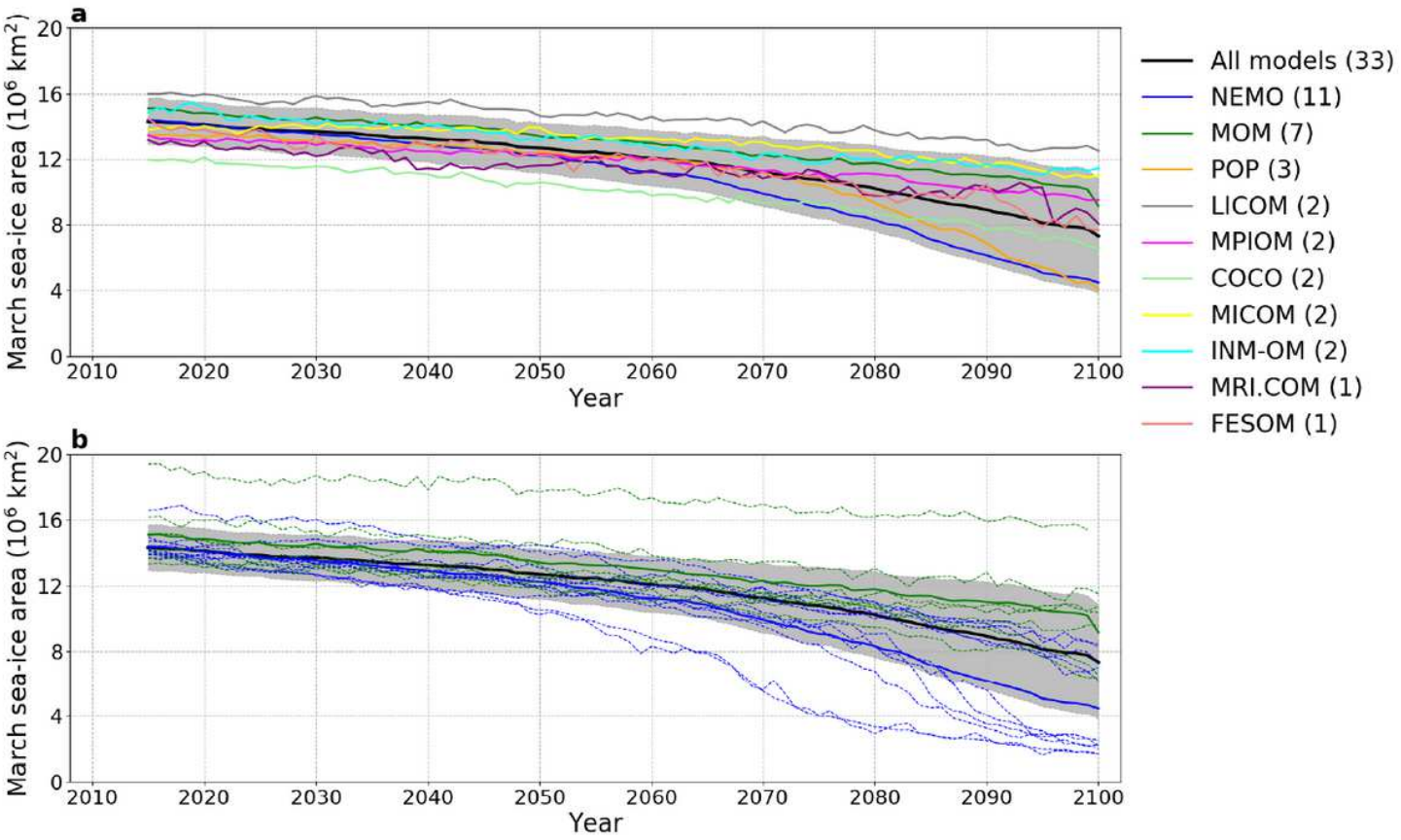

Figure 4

(a) Evolution of future March Arctic sea-ice area for the multi-model mean averaged over all models (thick black curve) and averaged over all models including the same ocean component (coloured curves), based on the SSP5-8.5 scenario. (b) Same as (a) but with only the multi-model means averaged over models including the NEMO (solid blue) and MOM (solid green) ocean components, as well as the individual NEMO and MOM models represented as dashed blue and green lines, respectively. The gray shading is the standard deviation around the multi-model mean without selection. The number of models included in each multi-model averaging is indicated in brackets in the legend.

Supplementary Files

This is a list of supplementary files associated with this preprint. Click to download.

- DocquierCMIP6SI.pdf